Supplementary Materials:Dehydrogenation of propane to propylene using promoter-free hierarchical Pt/silicalite-*1* nanosheets

Wannaruedee Wannapakdee [1], Thittaya Yutthalekha [1], Pannida Dugkhuntod [1], Kamonlatth Rodponthukwaji [2], Anawat Thivasasith [1], Somkiat Nokbin [2], Thongthai Witoon [3], Sitthiphong Pengpanich [4] and Chularat Wattanakit [1,*]

[1] School of Energy Science and Engineering, Nanocatalysts and Nanomaterials for Sustainable Energy and Environment Research Network of NANOTEC, Vidyasirimedhi Institute of Science and Technology, Rayong 21210, Thailand; wannaruedee.w@vistec.ac.th (W.W.); t.yutthalekha@gmail.com (T.Y.); s15_pannida.d@vistec.ac.th (P.D.); anawat.t@vistec.ac.th (A.T.)

[2] Department of Chemistry, NANOTEC Center for Nanoscale Materials Design for Green Nanotechnology, and Center for Advanced Studies in Nanotechnology and Its Applications in Chemical, Food and Agricultural Industries, Faculty of Science, Kasetsart University, Bangkok 10900, Thailand; kamonlatth@gmail.com (K.R.); fscisknb@ku.ac.th (S.N.)

[3] Center of Excellence on Petrochemical and Materials Technology, Department of Chemical Engineering, Faculty of Engineering, Kasetsart University, Bangkok 10900, Thailand; fengttwi@ku.ac.th (T.W.)

[4] PTT Global Chemical Public Company Limited (PTTGC), Vibhavadi Rangsit Road, Chatuchak, Bangkok 10900; Sitthiphong.P@pttgcgroup.com (S.P.)

* Correspondence: chularat.w@vistec.ac.th; Tel.: +66(0)33014255

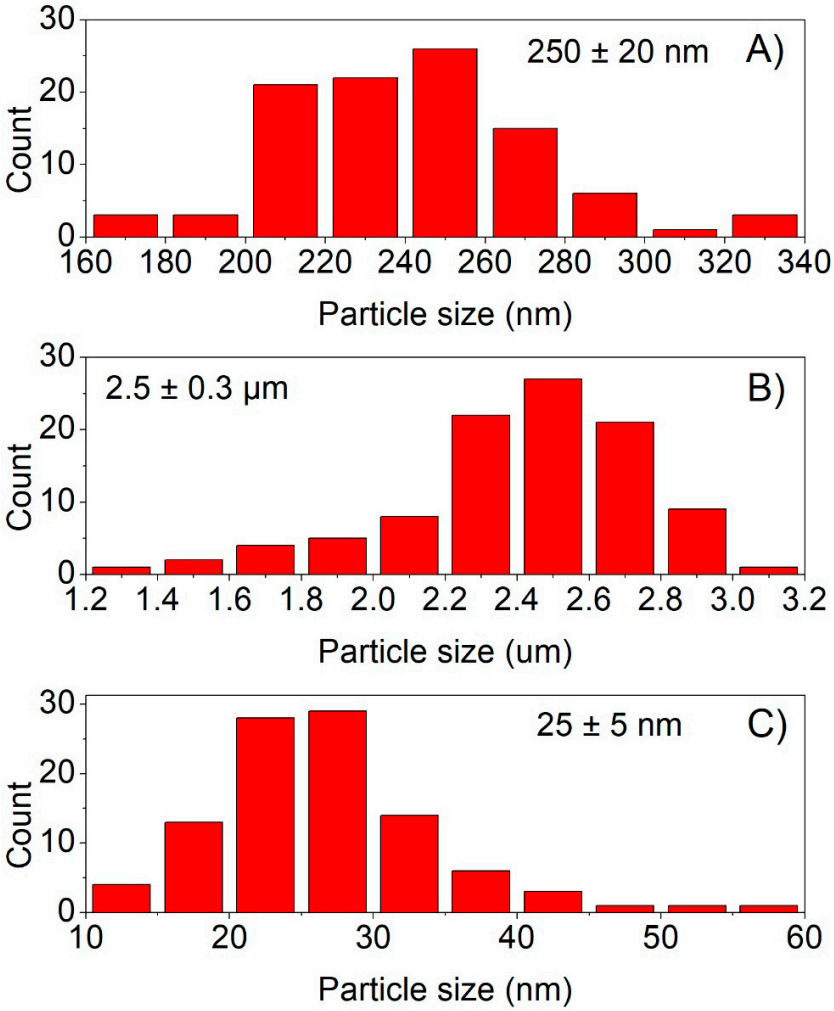

Figure S1. Particle size distribution of various supports: A) hierarchical silicalite-*1* nanosheets, B) conventional silicalite-*1*, and C) alumina.

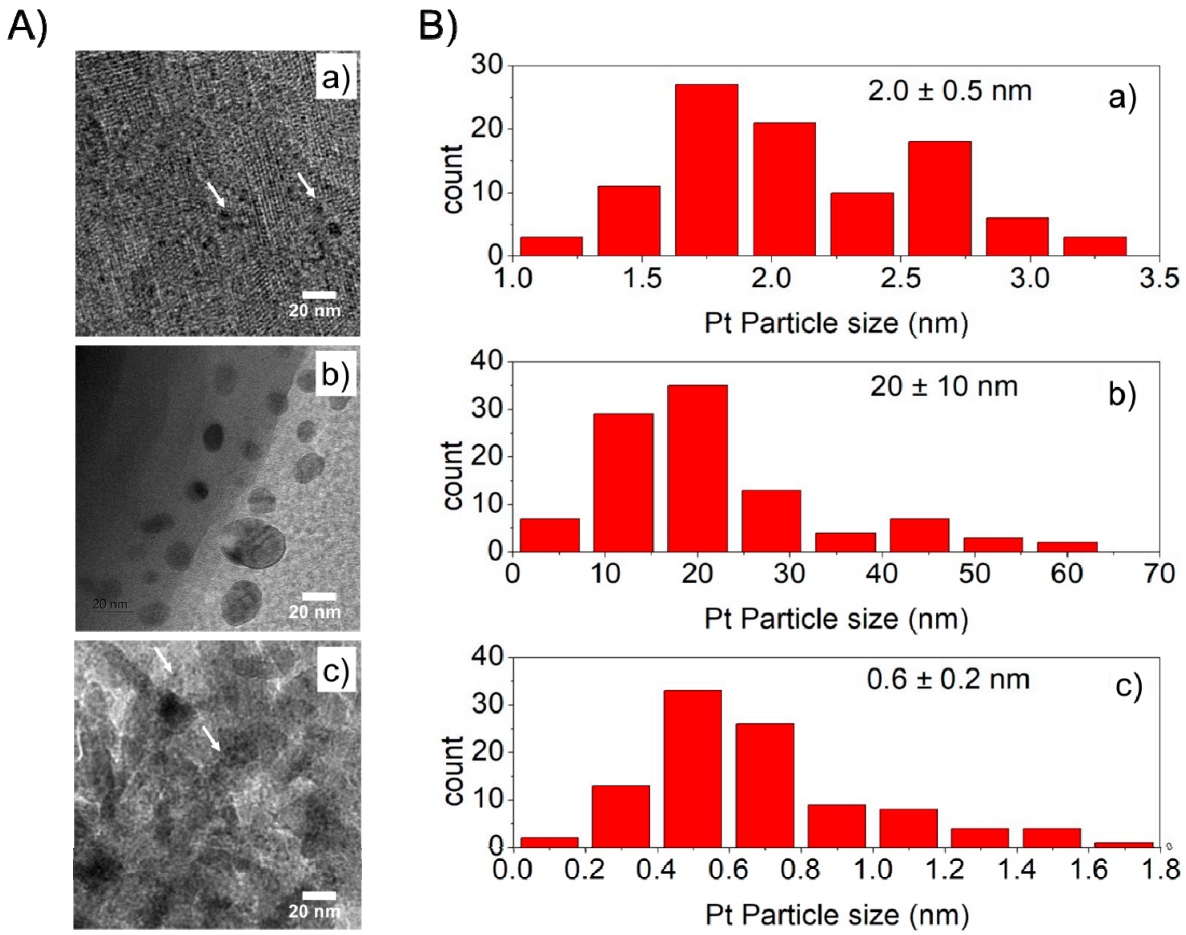

Figure S2. A) TEM images and B) Particle size distribution of Pt supported on various supports: a) hierarchical silicalite-*1* nanosheets, b) conventional silicalite-*1*, and c) alumina.

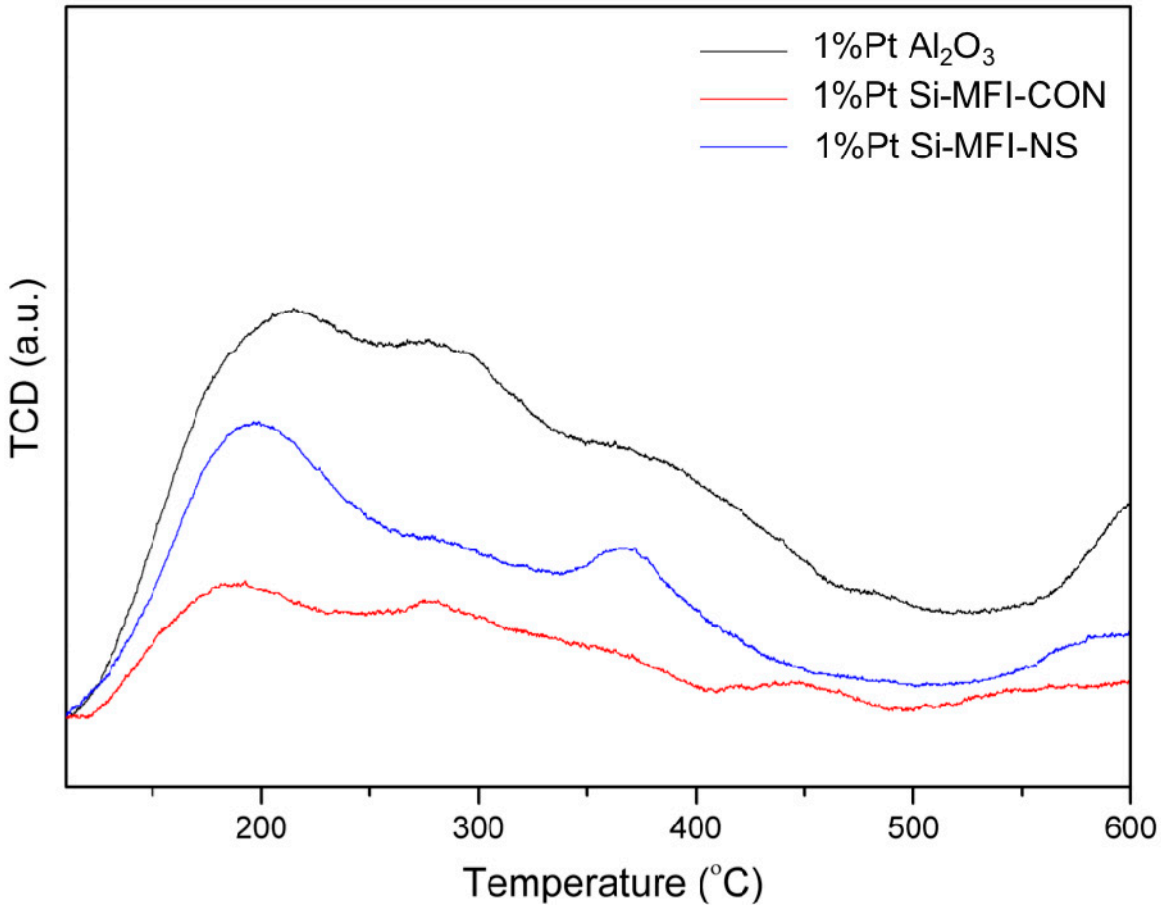

Figure S3. NH_3-TPD profiles of various supports, including 1wt%Pt hierarchical silicalite-*1* nanosheets (1%Pt-Si-MFI-NS), 1wt%Pt conventional silicalite-*1* (1%Pt-Si-MFI-CON) and 1%Pt alumina (Al_2O_3) (1%Pt-Al_2O_3).

Table S1. Summary of the contribution of Pt species[a].

Sample	[a]**Pt^0/Pt^{2+}**
1%Pt-Si-MFI-NS	1.11
1%Pt-Si-MFI-CON	1.09
1%Pt-Al_2O_3	-

[a]The ratio of Pt^0/Pt^{2+} calculates from the summation of peak area of Pt^0 divided by the summation of peak area of Pt^{2+}.

Table S2. Summary of metal size and the percentage of metal distribution of Pt supported catalysts obtained by H_2 chemisorption technique.

Entry	Sample	Metal size (nm)	Metal Distribution (%)
1	1%Pt-Si-MFI-NS	4.38	21
2	1%Pt-Si-MFI-CON	17.84	6
3	1%Pt-Al_2O_3	1.85	61

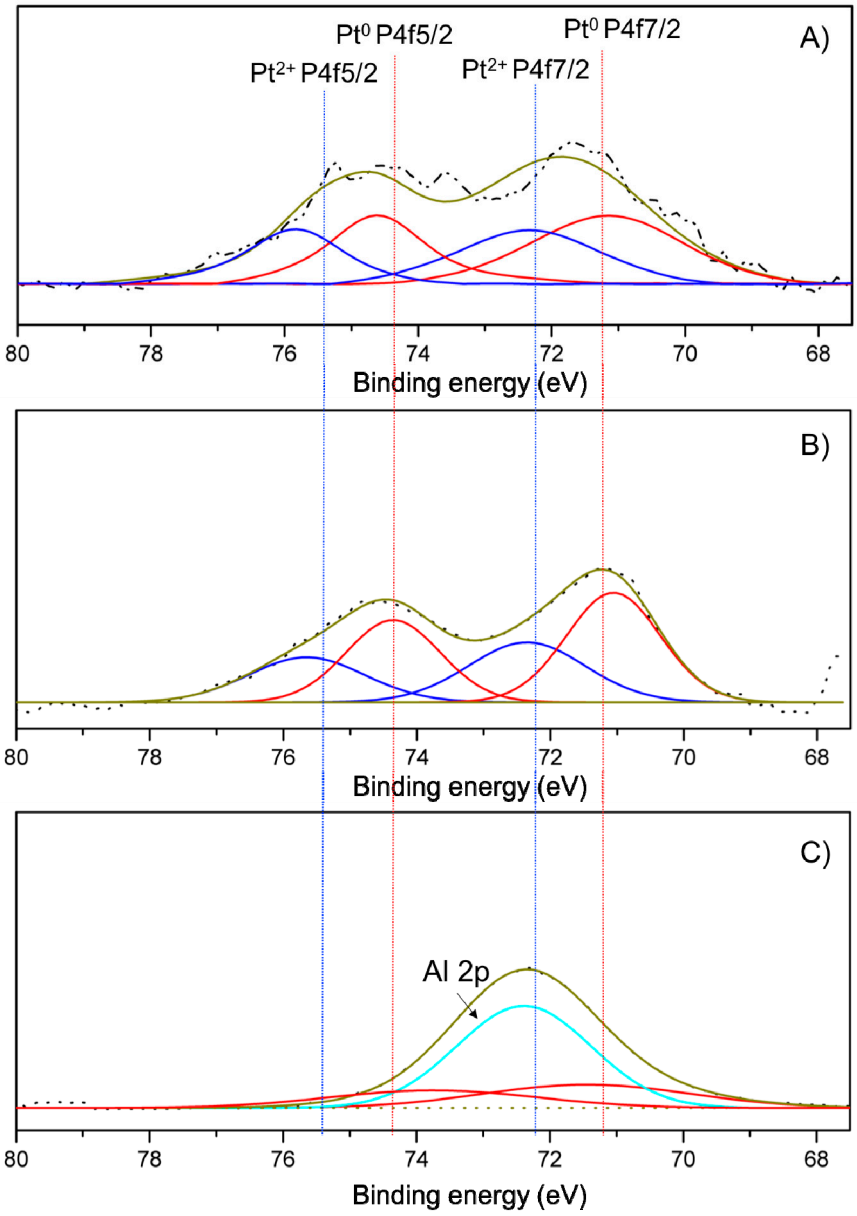

Figure S4. XPS spectra of Pt supported on different supports, including A) hierarchical silicalite-*1* nanosheets, B) conventional silicalite-*1*, and C) alumina.

XPS pretreatment condition: the sample was pretreated in the flow of Ar (50 ml.min^{-1}) at 150 °C for 1 h and then the temperature was ramped to 300 °C at 5°C.min^{-1} under the flow of 2% (v/v) H_2 in Ar (50 ml.min^{-1}) for 2h.

Diagnostic criteria for mass and heat transfer limitations in fixed bed reactors. In the gas-solid catalytic system, the performance of catalysts should be conducted in the kinetic regime in a fashion that gradients due to heat and mass transfer could be excluded. In this study, the heat and mass transfer limitations were checked for propane dehydrogenation to propylene at reaction temperature of 550 °C and atmospheric pressure. The experimental data were examined for possible intraparticle and interphase mass transfer by evaluating the Weisz-Prater criterion and Mears criterion, respectively,[1, 2] while the role

of interphase heat transfer and combined interphase and intraparticle heat and mass transfer was assessed by Mears criteria.[1, 2]

1.) Weisz-Prater criterion for internal diffusion

If $\frac{-r_A \rho_c R^2}{D_{pore,eff} C_{AS}} < 1$, then the effects of internal mass transfer can be neglected.

$-r_A$ = reaction rate = 0.008925 mole A kg_{cat}^{-1} s^{-1}

ρ_c = solid catalyst density bed = 1200 kg m^{-3}

R = catalyst particle radius, = 0.0002125 m

$D_{pore,eff}$ = effective pore diffusivity, 2.62x10^{-7} m^2 s^{-1}

Because the pore size of zeolites is slightly smaller than the mean free path, collisions with other molecules and with the wall are both important, and the diffusivity in the pore is predicted by combining the reciprocals of the bulk and Knudsen diffusivities. The details for the calculation of effective pore diffusivity are found from.[3]

$$\frac{1}{D_{pore,eff}} = \frac{1}{D_{AB,eff}} + \frac{1}{D_{K,eff}}$$

$$D_{AB,eff} = \frac{0.001858 T^{\frac{3}{2}} \left(\frac{1}{M_A} + \frac{1}{M_B} \right)^{\frac{1}{2}}}{P \sigma_{AB}^{\ 2} \Omega_D} \text{ x } \frac{\varepsilon}{\tau}$$

$\varepsilon =$ porosity = 0.4

$\tau =$ tortuosity = 3

$$D_{K,eff} = 9{,}700 r \sqrt{\frac{T}{M_i}} \text{ x } \frac{\varepsilon}{\tau}$$

$r =$ pore radius = 0.5 x 10^{-9} m

C_{AS} = bulk gas concentration of A = 7.88 mol m^{-3}

The highest value of $\frac{-r_A \rho_c R^2}{D_{pore,eff} C_{AS}}$ from our experiments was 0.234. Because the risk of internal diffusion limitation is indicated by $\frac{-r_A \rho_c R^2}{D_{pore,eff} C_{AS}} \geq 1$, the internal mass transfer limitation could be excluded in this study.

2.) Mears Criterion for external diffusion

If $\frac{-r_A \rho_b R n}{k_c C_{Ab}} < 0.15$, then the effects of external mass transfer cam be neglected.

$-r_A$ = reaction rate = 0.008925 mole A kg_{cat}^{-1} s^{-1}

ρ_b = bulk density of catalyst bed = 720 kg m^{-3}

R = catalyst particle radius, = 0.0002125 m

n = reaction order = 1

k_c = mass transfer coefficient = 0.299 = m s^{-1}

C_{Ab} = bulk gas concentration of A = 7.88 mol m^{-3}

Note that the Reynold number is low and the mass transfer coefficient (k_c) is calculated from the following equation [3]:

$$\mathrm{Sh} = \frac{2k_c R}{D_{eff}} = (4.0 + 1.21\mathrm{Pe}^{\frac{2}{3}})^{\frac{1}{2}}$$

Where Pe is Peclet number

The highest value of $\frac{-r_A \rho_b Rn}{k_c C_{Ab}}$ from our experiments was 0.000578. Because the risk of external diffusion limitation is indicated by $\frac{-r_A \rho_b Rn}{k_c C_{Ab}} \geq 0.15$, the external mass transfer limitation could be excluded in this study.

3.) Mears Criterion for external (interphase) heat transfer

If $\frac{|-\Delta H| - r_A \rho_b RE}{hT_b^{\,2} R_g} < 0.15$, then the effects of interphase heat transfer cam be neglected.

ΔH = heat of reaction = 124,000 J mole^{-1}

$-r_A$ = reaction rate = 0.008925 mole A kg$_{cat}^{-1}$ s^{-1}

ρ_b = bulk density of catalyst bed = 720 kg m^{-3}

R = catalyst particle radius = 0.0002125 m

h = heat transfer coefficient = 275.38 W m^{-2} K^{-1}

R_g = gas constant = 8.314 J mole^{-1} K^{-1}

The highest value of $\frac{|-\Delta H| - r_A \rho_b RE}{hT_b^{\,2} R_g}$ obtained with data from our experiments was 0.015. As the risk of interphase heat transfer limitation is indicated by $\frac{|-\Delta H| - r_A \rho_b RE}{hT_b^{\,2} R_g} \geq 0.15$, the interphase heat transfer limitation could be excluded in this study.

4.) Mears Criterion for combined interphase and intraparticle heat and mass transfer

If $\frac{-r_A \rho_b R^2}{C_{Ab} D_{pore,eff}} < \frac{1 + 0.33\gamma\chi}{|n - \gamma_b \beta_b|(1 + 0.33n\omega)}$, then the effects of combined interphase and intraparticle heat and mass transfer cam be neglected.

γ = Arrhenius number = $\frac{E}{R_g T_s}$

γ_b = Arrhenius number = $\frac{E}{R_g T_b}$

β_b = heat generation function = $\frac{(-\Delta H_r) D_{pore,eff} C_{Ab}}{\lambda T_b}$

E = activation energy = 121,336 J mole^{-1}

λ = catalyst thermal conductivity = 0.15 W m^{-1} K^{-1}

χ = Damköhler number for interphase heat transport = $\frac{(-\Delta H_r) - r_A \rho_b R}{hT_b}$

$\omega =$ Damköhler number for interphase mass transport = $\dfrac{-r_A \rho_b R}{k_c C_{Ab}}$

The highest value of $\dfrac{-r_A \rho_b R^2}{C_{Ab} D_{pore,eff}}$ obtained with data from our experiments was 0.14, while the value of $\dfrac{1+0.33\gamma\chi}{|n-\gamma_b\beta_b|(1+0.33n\omega)}$ was 1.053 which indicated that interphase and intraparticle heat and mass transfer limitation could be excluded in the present study.

Computational details. Models of the catalyst were presented by the 25T quantum cluster taken from the MFI zeolite lattice structure.[4] In the 25T model, the dangling bonds of surface oxygen atoms are terminated by H atoms at a distance of 1.47 Å[5-8] and the Si–H bonds are aligned in the directions of Si–O bonds of the MFI structure. In order to generate the "Q3" and "Q4" species in the MFI zeolite, the additional silanol groups were introduced into the 25T cluster. The Q3 species were modeled by adding four-silanol groups on the Si atoms at Si3, Si5, Si8, and Si10 positions as can be seen in the top view of MFI zeolite (Q3-MFI), whereas in the Q4 species four-silanol groups were added at Si9, Si11, Si15, and Si16 positions in the side view of MFI zeolite (Q4-MFI) (see Figure S5). Moreover, the modification of metal supported catalyst models was constructed by adding Pt_4 metal cluster. For the Q3-MFI, the Pt_4 clusters were stabilized on MFI zeolite by the interaction between Pt_4 cluster and four silanol groups, whereas in the Q4-MFI model the Pt_4 can be stabilized by the interaction between Pt_4 cluster and three O atoms of the framework. All calculations were performed using GAUSSIAN 09 code[9] with the M06-2X density functional.[10] The effective core potentials (ECP)[11] was selected for the basis set of Pt atoms while the basis set of 6-31G(d,p) was employed for the remaining atoms. During geometry optimizations, the 25T active region with Pt_4 cluster and the adsorbates were allowed to relax while the remaining terminated H atoms were fixed at their crystallographic coordinates. The triplet spin state was applied for the Pt_4 cluster doped on Q3- and Q4-MFI model. After the optimization, the binding energy (ΔE_B) and adsorption energy (ΔE_{ads}) in the reaction were calculated by the following equation:

$$\Delta E_B = E_{Pt4\text{-}MFI} - (E_{Pt4} + E_{MFI}) \quad (1)$$

where E_B is the binding energy of the Pt_4 cluster supported on the MFI model, $E_{Pt4\text{-}MFI}$ is the electronic energy of the isolate Pt_4/Qn-MFI (Qn = Q3 or Q4 species of MFI), E_{Pt4} is the electronic energy of the isolate Pt_4 cluster, E_{MFI} is the electronic energy of the isolate Qn-MFI framework

$$\Delta E_{ads} = E_{complex} - (E_{Pt4\text{-}MFI} + E_{adsorbate}) \quad (2)$$

where E_{ads} is the adsorption energy of the adsorbate molecule (propane or propylene) on the Pt_4/Qn-MFI, $E_{complex}$ is the electronic energy of the adsorbate complex on Pt_4/Qn-MFI, $E_{Pt4\text{-}MFI}$ is the electronic energy of the isolate Pt_4/Qn-MFI, and $E_{adsorbate}$ is the electronic energy of the propane or propylene molecule. The binding energy the Pt_4 cluster supported on the MFI and adsorption energy of propylene are in good agreement with those reported in previous literatures [8, 12, 13]

The optimization geometrical parameters were reported in Table S3. Moreover, partial charges were also determined by the natural atomic orbital (NAO)[14] in Table S4.

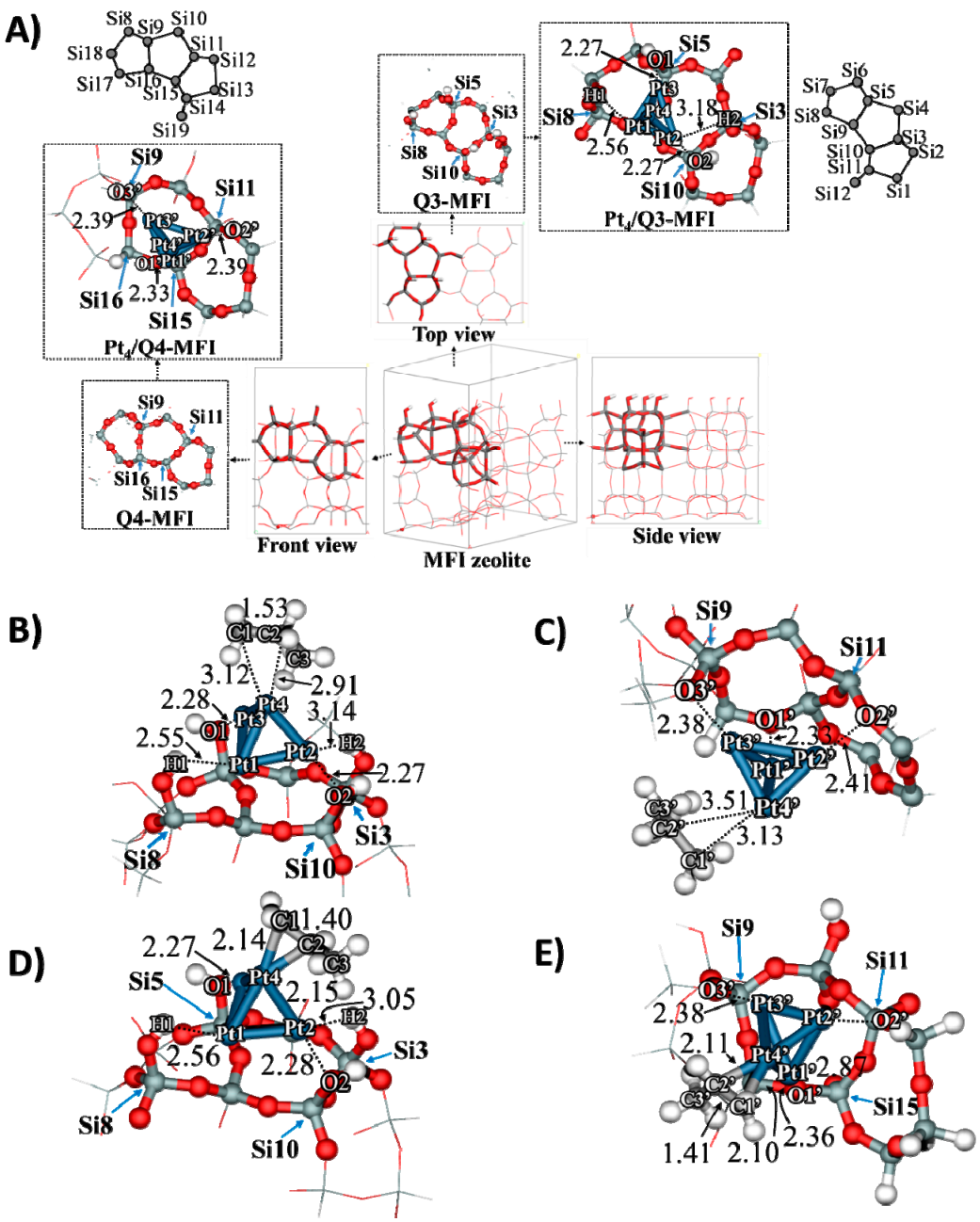

Figure S5 A) The 25T models of Q3 and Q4 species in MFI zeolite as well as Pt_4 cluster embedded on Q3-MFI and Q4-MFI zeolite models, the optimized structure of propane on B) Pt_4/Q3-MFI and C) Pt_4/Q4-MFI zeolite, and the optimized structures of propylene on D) Pt_4/Q3-MFI and E) Pt_4/Q4-MFI zeolites.

Table S3. Selected geometrical parameters of Pt_4/Q3-MFI and Pt_4/Q4-MFI zeolites and the corresponding adsorption complexes including isolated Pt_4, propane and propylene.

	Isolated molecules	Pt_4/Q3-MFI
Distances (Å)		
Pt1-Pt2	2.62	2.65
Pt1-Pt3	2.62	2.63
Pt1-Pt4	2.60	2.56
Pt2-Pt3	2.83	3.17
Pt2-Pt4	2.62	2.56
Pt3-Pt4	2.62	2.57
Pt1-H1	-	2.56
Pt2-H2	-	3.18
Pt2-O2	-	2.27
Pt3-O1	-	2.27

	Isolated molecules	Pt_4/Q4-MFI
Distances (Å)		
Pt1'-Pt2'	2.62	2.62
Pt1'-Pt3'	2.62	2.65
Pt1'-Pt4'	2.60	2.57
Pt2'-Pt3'	2.83	3.16
Pt2'-Pt4'	2.62	2.56
Pt3'-Pt4'	2.62	2.57
Pt1'-O1'	-	2.33
Pt2'-O2'	-	2.39
Pt3'-O3'	-	2.39

	Isolated molecules	*Propane/* Pt_4/Q3-MFI
Distances (Å)		
Pt1-Pt2	2.62	2.64
Pt1-Pt3	2.62	2.63
Pt1-Pt4	2.60	2.55
Pt2-Pt3	2.83	3.15
Pt2-Pt4	2.62	2.57
Pt3-Pt4	2.62	2.58
Pt1-H1	-	2.55
Pt2-H2	-	3.14
Pt2-O2	-	2.27
Pt3-O1	-	2.28
C1-C2	1.53	1.53
C2-C3	1.53	1.53

	Isolated molecules	*Propane/* Pt_4/Q4-MFI
Distances (Å)		
Pt1'-Pt2'	2.62	2.63
Pt1'-Pt3'	2.62	2.64
Pt1'-Pt4'	2.60	2.57
Pt2'-Pt3'	2.83	3.08
Pt2'-Pt4'	2.62	2.55
Pt3'-Pt4'	2.62	2.58
Pt1'-O1'	-	2.33
Pt2'-O2'	-	2.41
Pt3'-O3'	-	2.38
C1'-C2'	1.53	1.53
C2'-C3'	1.53	1.53

	Isolated molecules	*Propylene/* Pt_4/Q3-MFI
Distances (Å)		
Pt1-Pt2	2.62	2.59
Pt1-Pt3	2.62	2.61
Pt1-Pt4	2.60	2.60
Pt2-Pt3	2.83	2.94
Pt2-Pt4	2.62	2.71
Pt3-Pt4	2.62	2.64
Pt1-H1	-	2.56
Pt2-H2	-	3.05
Pt2-O2	-	2.28
Pt3-O1	-	2.27

	Isolated molecules	*Propylene/* Pt_4/Q4-MFI
Distances (Å)		
Pt1'-Pt2'	2.62	2.63
Pt1'-Pt3'	2.62	2.66
Pt1'-Pt4'	2.60	2.59
Pt2'-Pt3'	2.83	2.56
Pt2'-Pt4'	2.62	2.64
Pt3'-Pt4'	2.62	3.02
Pt1'-O1'	-	2.36
Pt2'-O2'	-	2.87
Pt3'-O3'	-	2.38
C1'-C2'	1.33	1.41

C1-C2	1.33	1.40	C2'-C3'	1.50	1.51
C2-C3	1.50	1.51			

Table S4 Summarized partial charges determined by the natural atomic orbital (NAO)

	Isolated molecules	Pt_4/Q3-MFI		Isolated molecules	Pt_4/Q4-MFI
Charge (e)			*Charge (e)*		
Pt_4 cluster	0.000	-0.290	Pt_4 cluster	0.000	-0.252
Pt1	-0.043	-0.156	Pt1'	-0.043	-0.115
Pt2	0.043	0.031	Pt2'	0.043	0.022
Pt3	0.044	0.010	Pt3'	0.044	0.006
Pt4	-0.044	-0.175	Pt4'	-0.044	-0.164
O1	-1.119	-1.111	O1'	-1.289	-1.273
O2	-1.133	-1.119	O2'	-1.283	-1.267
H1	0.531	0.547	O3'	-1.280	-1.259
H2	0.539	0.550			

	Isolated molecules	*Propane/* Pt_4/Q3-MFI		Isolated molecules	*Propane/* Pt_4/Q4-MFI
Charge (e)			*Charge (e)*		
Pt_4 cluster	0.000	-0.344	Pt_4 cluster	0.000	-0.324
Pt1	-0.043	-0.128	Pt1'	-0.043	-0.103
Pt2	0.043	0.065	Pt2'	0.043	0.004
Pt3	0.044	0.065	Pt3'	0.044	-0.011
Pt4	-0.044	-0.346	Pt4'	-0.044	-0.213
O1	-1.119	-1.112	O1'	-1.289	-1.272
O2	-1.133	-1.117	O2'	-1.283	-1.267
H1	0.531	0.548	O3'	-1.280	-1.257
H2	0.539	0.550	C1'	-0.700	-0.682
C1	-0.700	-0.692	C2'	-0.475	-0.466
C2	-0.475	-0.478	C3'	-0.700	-0.684
C3	-0.700	-0.693	Propane	0.000	0.035
Propane	0.000	0.049			

	Isolated molecules	*Propylene/* Pt_4/Q3-MFI		Isolated molecules	*Propylene/* Pt_4/Q4-MFI
Charge (e)			*Charge (e)*		
Pt_4 cluster	0.000	-0.218	Pt_4 cluster	0.000	-0.162
Pt1	-0.043	-0.168	Pt1'	-0.043	-0.027
Pt2	0.043	0.040	Pt2'	0.043	-0.124
Pt3	0.044	0.062	Pt3'	0.044	-0.001
Pt4	-0.044	-0.152	Pt4'	-0.044	-0.011
O1	-1.119	-1.113	O1'	-1.289	-1.273
O2	-1.133	-1.112	O2'	-1.283	-1.285
H1	0.531	0.544	O3'	-1.280	-1.261
H2	0.539	0.546	C1'	-0.454	-0.559
C1	-0.454	-0.574	C2'	-0.221	-0.316
C2	-0.221	-0.283	C3'	-0.728	-0.689
C3	-0.728	-0.707	Propylene	0.000	-0.093

Propylene	0.000	-0.062

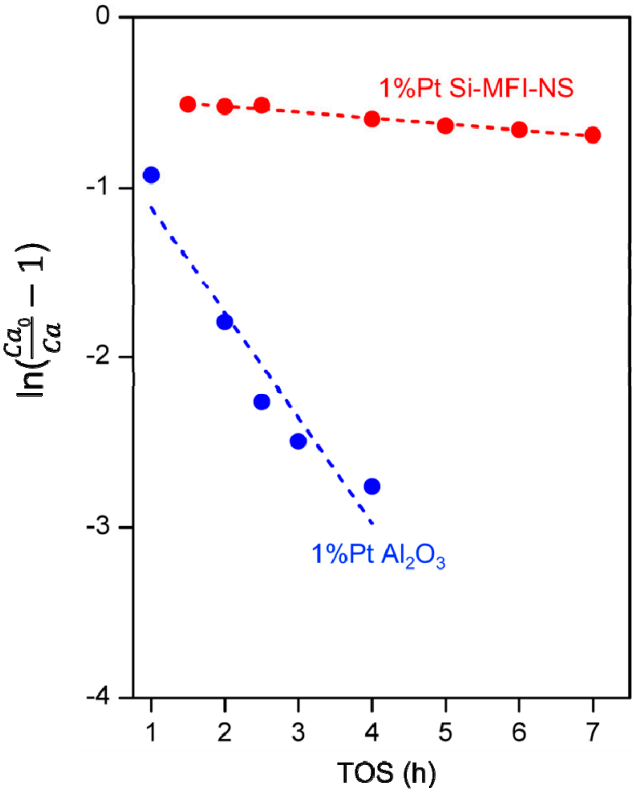

Figure S6 Deactivation rate of the 1%Pt alumina (Al_2O_3) (1%Pt-Al_2O_3) and the 1wt%Pt hierarchical silicalite-*1* nanosheets (1%Pt-Si-MFI-NS).

References

(1) D.E. Mears, Diagnostic criteria for heat transport limitations in fixed bed reactors, *J. Catal.*, **1971**, 20, 127–131.

(2) R.J. Madon, M. Boudart, Experimental criterion for the absence of artifacts in the measurement of rates of heterogeneous catalytic reactions, *Ind. Eng. Chem. Fundam.*, **1982,** 21, 438–447.

(3) W. McCabe, J. Smith, P. Harriott, Unit Operations of Chemical Engineering 7th ed. *McGraw-Hill*, New York, **2005**.

(4) E.M. Flanigen, J.M. Bennett, R.W. Grose, J.P. Cohen, R.L. Patton, R.M. Kirchner, J.V. Smith, Silicalite, a new hydrophobic crystalline silica molecular sieve, *Nature*, **1978,** 271, 512-516.

(5) B. Boekfa, P. Pantu, M. Probst, J. Limtrakul, Adsorption and Tautomerization Reaction of Acetone on Acidic Zeolites: The Confinement Effect in Different Types of Zeolites, *The J. Phys. Chem. C*, **2010,** 114, 15061-15067.

(6) T. Maihom, S. Wannakao, B. Boekfa, J. Limtrakul, Density functional study of the activity of gold-supported ZSM-5 zeolites for nitrous oxide decomposition, *Chem. Phys. Lett.*, **2013,** 556, 217-224.

(7) W. Panjan, J. Sirijaraensre, C. Warakulwit, P. Pantu, J. Limtrakul, The conversion of CO_2 and CH_4 to acetic acid over the Au-exchanged ZSM-5 catalyst: a density functional theory study, *PCCP.*, **2012,** 14, 16588-16594.

(8) M.N. Mikhailov, I.V. Mishin, L.M. Kustov, V.Z. Mordkovich, The structure and activity of Pt_6 particles in ZSM-5 type zeolites, *Catal. Today*, **2009,** 144, 273-277.

(9) G.W.T. M. J. Frisch, H. B. Schlegel, G. E. Scuseria, M. A. Robb, J. R. Cheeseman, G. Scalmani, V. Barone, B. Mennucci, G. A. Petersson, H. Nakatsuji, M. Caricato, X. Li, H. P. Hratchian, A. F. Izmaylov, J. Bloino, G. Zheng, J. L. Sonnenberg, M. Hada, M. Ehara, K. Toyota, R. Fukuda, J. Hasegawa, M. Ishida, T. Nakajima, Y. Honda, O. Kitao, H. Nakai, T. Vreven, J. A. Montgomery, Jr., J. E. Peralta, F. Ogliaro, M. Bearpark, J. J. Heyd, E. Brothers, K. N. Kudin, V. N. Staroverov, R. Kobayashi, J. Normand, K. Raghavachari, A. Rendell, J. C. Burant, S. S. Iyengar, J. Tomasi, M. Cossi, N. Rega, J. M. Millam, M. Klene, J. E. Knox, J. B. Cross, V. Bakken, C. Adamo, J. Jaramillo, R. Gomperts, R. E. Stratmann, O. Yazyev, A. J. Austin, R. Cammi, C. Pomelli, J. W. Ochterski, R. L. Martin, K. Morokuma, V. G. Zakrzewski, G. A. Voth, P. Salvador, J. J. Dannenberg, S. Dapprich, A. D. Daniels, Ö. Farkas, J. B. Foresman, J. V. Ortiz, J. Cioslowski, and D. J. Fox,, Gaussian 09, revision c.01; Gaussian, Inc.: Pittsburgh, PA, **2009**.

(10) Y. Zhao, D.G. Truhlar, Density Functionals with Broad Applicability in Chemistry, *Acc. Chem. Res.*, **2008,** 41, 157-167.

(11) M. Dolg, H. Stoll, H. Preuss, R.M. Pitzer, Relativistic and correlation effects for element 105 (hahnium, Ha): a comparative study of M and MO (M = Nb, Ta, Ha) using energy-adjusted ab initio pseudopotentials, *J. Phys. Chem.*, **1993,** 97, 5852-5859.

(12) L. Nykänen and K. Honkala, Density Functional Theory Study on Propane and Propene Adsorption on Pt(111) and PtSn Alloy Surfaces, *J. Phys. Chem. C*, **2011**, 1**15,** 9578-9586.

(13) M.-L. Yang, Y.-A. Zhu, C. Fan, Z.-J. Sui, D. Chen and X.-G. Zhou, Density functional study of the chemisorption of C1, C2 and C3 intermediates in propane dissociation on Pt(111), *J. Mol. Catal. A Chem.*, **2010,** 321**,** 42-49.

(14) A. E. Reed, L. A. Curtiss and F. Weinhold, Intermolecular interactions from a natural bond orbital, donor-acceptor viewpoint, *Chem. Rev.*, **1988,** 88**,** 899-926.